Acta Neuropathologica Communications

RESEARCH Open Access

Aqueous extractable nonfibrillar and sarkosyl extractable fibrillar Alzheimer's disease tau seeds have distinct properties

Anastasie Mate de Gerando[1,2], Anita Khasnavis[1], Lindsay A. Welikovitch[1], Harshil Bhavsar[1], Calina Glynn[1,2], Noe Quittot[1], Romain Perbet[1] and Bradley T. Hyman[1,2*]

Abstract
Pathological tau fibrils in progressive supranuclear palsy, frontotemporal dementia, chronic traumatic encephalopathy, and Alzheimer's disease each have unique conformations, and post-translational modifications that correlate with unique disease characteristics. However, within Alzheimer's disease (AD), both fibrillar (sarkosyl insoluble (AD SARK tau)), and nonfibrillar (aqueous extractable high molecular weight (AD HMW tau)) preparations have been suggested to be seed-competent. We now explore if these preparations are similar or distinct in their in vivo seeding characteristics. Using an in vivo amplification and time-course paradigm we demonstrate that, for AD HMW and AD SARK tau species, the amplified material is biochemically similar to the original sample. The HMW and SARK materials also show different clearance, propagation kinetics, and propagation patterns. These data indicate the surprising co-occurrence of multiple distinct tau species within the same AD brain, supporting the idea that multiple tau conformers – both fibrillar and nonfibrillar- can impact phenotype in AD.

Keywords Alzheimer, Tau, Seeding, Spreading, Kinetics

Introduction

Tau accumulates in several neurodegenerative diseases that have unique phenotypes including Alzheimer's disease (AD), progressive supranuclear palsy (PSP), frontotemporal dementia, and corticobasal degeneration (CBD). These are distinguished by different cryo-EM-defined structures [60], different isoforms and post-translational modifications [6, 70], and different regional distributions [14, 21, 50]. Within AD, tau is present in more than one biochemically distinct, bioactive form, including aqueous extractable high molecular weight tau (HMW) [29, 48, 64] and sarkosyl insoluble (SARK) paired helical filament (PHF) [10, 14, 34, 36] both of which support templated misfolding and seeding in vitro. The aqueous soluble tau is further purified over a size exclusion column, collecting early fractions that are likely oligomeric species, and which have been shown by electron microscopy (EM) and atomic force microscopy to contain amorphous rather than fibrillar aggregates [44, 48, 64]. The fibrillar tau is isolated using a standard sarkosyl insoluble protocol, and this material contains classical paired helical filament fibrils [44, 48]. Mass spectrometry analysis of the two preparations reveals an overlapping but distinct set of post-translational modifications, with the sarkosyl preparation containing nearly twice as many post-translational alterations as HMW tau [44, 70].

*Correspondence:
Bradley T. Hyman
bhyman@mgh.harvard.edu
[1]Department of Neurology, Massachusetts General Hospital, Boston, MA, USA
[2]Harvard Medical School, Cambridge, MA, USA

We now explore if HMW and SARK tau should be considered two distinct forms of AD tau in the context of their behavior in vivo. We therefore tested whether the kinetics of propagation differ after injection of these conformationally distinct but molecularly similar forms of tau, and if the propagated forms of tau after corruption of endogenous tau are phenotypically similar to the original injected material.

We used the wild-type 6 human tau isoform-expressing hTau mouse model [4] to study the kinetics of tau seeding and propagation in vivo. Time-course experiments revealed that, despite rapid clearance of AD HMW and AD SARK tau from the injection site within 2.5 weeks, both injected exogenous tau seeds have recruited endogenous tau to a bioactive form and triggered visible tau pathology by 1 month after injection. While AD HMW tau-induced tau pathology spreads faster to the entorhinal cortex, only AD SARK tau-induced pathology developed sarkosyl-insoluble aggregates 3 months after injection. Importantly, this in vivo amplification system is consistent with the templated misfolding hypothesis with AD HMW tau generating only PBS-extractable tau seeds and only AD SARK tau producing sarkosyl-insoluble tau seeds. These data emphasize the distinct nature of HMW and SARK tau derived from the same AD brain accounting for their different kinetics regarding tau pathology progression, important features to consider for anti-tau drug development and therapeutic time window optimization.

Methods

Human tissue

Approximatively 5 g of frozen frontal cortex corresponding to Brodmann Area 7 (BA 7), from an AD case we used in a previous study [48], was dissected and kept at -80 °C until processing for either HMW or SARK Tau extraction. The AD case was selected from the Massachusetts Alzheimer's Disease Research Center using the following criteria: (i) clinical diagnosis of dementia due to probable AD; (ii) postmortem confirmation of AD diagnosis; (iii) Braak stage V determined by total Tau immunostain and Bielchowsky's silver stain of NFTs; (iv) the least possible comorbidities (Table 1). Human brain tissue was collected with informed consent and approval of local institutional review boards at Massachusetts General Hospital.

HMW Tau extraction

Frozen human cortical grey matter (5 g) was processed for high molecular weight tau extraction as previously described [48]. Briefly, tissue was Dounce homogenized in 5 volumes to weight (v/w) with 30 strokes at 70% power in PBS and protease inhibitor (#5871, Cell signaling) homogenization buffer. After centrifugation at 10,000 g for 10 min, the PBS extractable supernatant was collected and loaded on a SEC column (HiLoad 16/600 Superdex 200 pg column, no. 28-9893-35, GE Healthcare) for further separation of PBS extracts per molecular weight. Fractions corresponding to high molecular weight tau (elution volumes 40, 42.5 and 45 ml) were pooled and centrifuged at 150,000 g for 30 min at 4 °C (MLA-130 fixed-angle rotor, Beckman) to concentrate the sample (AD HMW tau) and stored at -80 °C until further use.

SARK Tau extraction

Frozen human cortical grey matter (5 g) was processed for sarkosyl-insoluble tau protein extraction as previously described [48]. Briefly, tissue was Dounce homogenized in 9 v/w high salt buffer (10 mM Tris pH 7.4, 10% sucrose, 0.8 M NaCl, 1 mM EDTA, 0.1% sarkosyl and 1X protease/phosphatase inhibitor cocktail, #5872, Cell signaling) with 15 strokes at 70% power. After centrifugation at 10,000 g for 10 min the supernatant was collected and a solution of 25% sarkosyl was added to get a final concentration of 1% sarkosyl and was incubated for 1 h under agitation at room temperature (RT). After several high-speed centrifugations and PBS wash steps, the pellet was resuspended in PBS 1X and sonicated 60 short pulses before centrifugation 30 min at 10,000 g at 4 °C. The final supernatant contained the sarkosyl-insoluble Tau species (AD SARK tau) and were stored at -80 °C until further use. AD SARK tau samples were extemporaneously sonicated for 60 short pulses on power 2 on ice using a hand-held sonicator as recommended in the literature [36, 51] before injection.

Tau immunodepletion

To verify the Tau-driven effects of the AD HMW and AD SARK samples, we immunodepleted total tau using HT7 antibody (MN1000, Invitrogen) and PureProteome Protein G Magnetic Beads (Millipore Corp, LSKMAGG02) as described previously [48]. The process was repeated three times total for successful total tau

Table 1 AD case demographic and characteristics used in this study

#ADRC	Brain region	Age at death	Sex	NPDX1	NPDX2	Braak Stage	Thal Stage
2399	BA 7	74	Male	Alzheimer's Disease Neuropathological Changes (ADNC)	Cerebrovascular Disease (CVD)	V	5

immunodepletion. The success of the tau immunodepletion was confirmed by total tau western blot and tau seeding assay (Additional File 1: Supplementary Fig. 3a-b).

Denaturing and non-denaturing blots

Each SARK and HMW tau sample was run on a denaturing western blot (WB) to quantify total tau monomer equivalents as previously described [48]. For AT8 immunoblotting, 1.5 µg of total tau monomer equivalents were loaded onto the gel for each sample, and the membrane was incubated for 5 min in boiling tris-buffer saline (TBS) before overnight primary antibody incubation (Additional File 2: Supplementary Table 1).

For native gels, the Novex® NativePAGE™ Bis-Tris gel system (ThermoFisher) was used as per manufacturer's protocol. For each sample, 0.05 µg of total tau monomer equivalents were loaded onto the gel. After electrophoresis, proteins were transferred to a PVDF membrane using the iBlot 2 gel transfer device. The membrane was quickly washed in methanol to remove the excess blue, incubated 5 min in 8% acetic acid to fix the proteins, then rinsed in deionized water and air-dried prior to incubation in blocking buffer (5% non-fat dried milk diluted in TBS-triton) for 1 h at RT. The membrane was then incubated overnight at 4 °C with anti-total tau primary antibody solution (1: 5000, DAKO A0024). After 1 h incubation at RT in the corresponding HRP secondary antibody solution, blots were imaged using high-sensitivity SuperSignal™ West Pico PLUS Chemiluminescent Substrate (ThermoFisher) on a chemiluminescent BioRad Chemi-Doc Imaging System.

Immuno-gold negative stain electron microscopy

For electron microscopy (EM), 0.1 µg monomeric equivalent of total tau was loaded onto glow-discharged F/C 300 mesh Nickel grids for two minutes as previously described. Immuno-gold labeling was carried out as previously described [35], where floating the grid on a drop of blocking buffer (PBS+0.1% gelatin) for 10 min followed sample application. Grids were then floated on a drop with the C-terminal antibody Tau46 (Cell Signaling #4019) diluted 1:20 in blocking buffer for 1–2 h at RT. Grids were washed three times by floating on a drop of blocking buffer for five minutes each, then floated on a drop of undiluted gold-conjugated secondary antibody for 1 h and washed twice with PBS and twice with water before staining for 2 min with 2% uranyl acetate. Images were taken on a ThermoFisher Scientific T12 electron microscope at the Harvard Medical School Molecular Electron Microscopy Suite (HMS MEMS) at magnifications of 26,000x.

In vivo experiments

Three-month-old hTau transgenic mice of either sex (B6.Cg-*Mapt*$^{tm1(EGFP)Klt}$ Tg(MAPT)8cPdav/J, purchased from Jax and bred in-house) expressing the 6 human tau isoforms on a mouse tau null background (n=4–6/group) were used for time-course experiments (Additional File 1: Supplementary Fig. 1a). Three-month-old TauKO littermates devoid of any human or murine tau were used as controls. Mice underwent anesthesia with 1.5% (vol/vol) isoflurane and were placed onto a stereotaxic frame, ophthalmic ointment was placed on the eyes and lidocaine (lidocaine hydrochloride, 2 mg/kg) subcutaneously administered under the scalp skin before the beginning of surgery. Mice were bilaterally injected into the CA1 of the dorsal hippocampus (anteroposterior −2.4 mm from bregma, mediolateral +/- 1.5 mm from midline and dorsoventral −1.6 mm from the skull surface) using a 33-gauge blunt tip needle linked to a Hamilton syringe. Each mouse received 1 µg AD HMW or AD SARK tau diluted in PBS (2.33 µl/site) at a flow rate of 0.2 µl/min. AD HMW and AD SARK total tau concentrations were quantified by western blot (WB) using a calibration curve as previously described [48]. PBS alone was used as control for injections. An additional subset of hTau mice (n=2–3/group) were injected with AD HMW and AD SARK samples immunodepleted for total tau. To test the influence of amyloid pathology triggering factors on tau seeds bioactivity, we generated triple transgenic APPxhTau mice expressing the 6 human tau isoforms and mutated human APP and PS1 on a murine tau null background by crossing hTau mice with APP/PS1 mice, and injected them with either AD HMW tau or PBS (n=3/group) at 3 months of age. After intracerebral injection, the skin was sutured, and buprenorphine (buprenorphine hydrocholoride 0.05 mg/ml) subcutaneously administered every 12 h for 72 h. Post-surgery analgesia was further ensured by the administration of acetaminophen (300 mg/kg) in drinking water for 72 h.

Mice were euthanized with CO_2 and transcardially perfused with ice-cold PBS for 5 min at 20 ml/min at 6 different time-points including 1 day, 3 days, 1 week, 2.5 weeks, 1 month and 3 months after injection. The brains were removed, and the hemispheres separated. The left hemisphere was post-fixed for 24 h in 4% paraformaldehyde (PFA) and cryoprotected in 30% sucrose in PBS for 72 h before sectioning. Coronal sections (40 µm-thick) were sliced using a freezing microtome and were collected at 400 µm intervals. The right hemisphere was dissected to isolate the hippocampus and peri-/entorhinal cortices from the rest of the brain, frozen on dry ice and kept at -80 °C until further processing.

All animal care, housing and experiments were performed in compliance with guidelines established by the Massachusetts General Hospital institutional animal care

and use committee and in accordance with the National Institutes of Health Guide for the Care and Use of Laboratory Animals.

Mouse brain homogenization

The fresh frozen hippocampi were homogenized 30 strokes at power 70% in 8 v/w PBS containing 1X protease inhibitor (#5871, Cell signaling) using a 1 ml glass homogenizer. For each animal, peri-/entorhinal cortices were homogenized in 200 µl PBS/protease inhibitor buffer. The homogenates were then centrifuged 10 min at 10,000 g at 4 °C, the PBS extractable supernatants collected and stored at -80 °C until further use. Pellets were processed using a modified sarkosyl-extraction protocol. Briefly, each pellet was homogenized in 1 ml high salt buffer (10 mM Tris pH 7.4, 10% sucrose, 0.8 M NaCl, 1 mM EDTA, 0.1% sarkosyl and 1X protease/phosphatase inhibitor cocktail, #5872, Cell signaling) with 20 strokes at 70% power. After centrifugation at 10,000 g for 10 min the supernatant was collected and a solution of 25% sarkosyl was added to get a final concentration of 1% sarkosyl and let incubating for 1 h under agitation at RT. The mixture was then centrifuged 60 min at 300,000 g at 4 °C, the supernatant discarded, and the pellet resuspended in 20 µl PBS and stored at -80 °C until further use (Additional File 1: Supplementary Fig. 2a).

A total of 2 PBS extractable and 2 sarkosyl-insoluble samples were generated per animal including the hippocampus and peri-/entorhinal cortices. Total protein concentrations were determined by BCA analysis using the manufacturer's protocol (ThermoFisher), and subsequent experiments were performed normalizing on total protein concentration.

In vitro seeding assay

To evaluate seeding activity in mouse brain homogenates after AD tau injection, we used the widely used FRET-biosensor assay [29, 39] with HEK cells stably expressing the repeat domain of tau with the P301S mutation conjugated to either cyan fluorescent protein (CFP) or yellow fluorescent protein (YFP) (TauRD-P301S-CFP/YFP). Cells were plated on 96-well plates (Costar, previously coated with 1:20 poly-D-lysine) at a density of 20,000 cells per well and cultured 24 h at 37 °C, 5% CO2 in Dulbecco's Modified Eagle Medium (DMEM), 10% fetal bovine serum (FBS) and 1% penicillin-streptomycin. PBS extractable and sarkosyl-insoluble mouse brain hippocampal, and entorhinal extracts (1 µg total protein quantified by BCA per well) were incubated with 1% lipofectamine (Invitrogen) in opti-MEM (ThermoFisher, final volume of 50 µl per well) for 20 min at RT before being added to the cells. After 24 h, cells were collected, fixated in 2% PFA for 20 min in the dark and resuspended in 150 µl per well PBS for subsequent flow cytometer analysis of seeding i.e. FRET signal (MACSQuant VYB, Miltenyi) as previously described [29, 48]. Within each time-point, integrated FRET densities (IFD) were corrected to the PBS-injected animals. Each sample was loaded in triplicates and the average of 3 independently run experiments was plotted on the graphs.

Dotblots for pTau screening

We used dotblots to screen for tau phospho-epitopes in our different injection paradigms. For each sample, 0.01 µg total protein (quantified by BCA) was loaded onto a nitrocellulose membrane in a total volume of 50 µl containing 1X NuPAGE sample reducing agent (Thermo Fisher) and 1% sodium dodecyl sulfate (SDS) diluted in PBS 1X after denaturation at 95 °C for 10 min. After letting samples sit on the membranes for 30 min at RT, membranes were incubated 30 min at RT with agitation in Intercept blocking buffer (Licor), then incubated overnight at 4 °C in primary antibody solutions (Additional File 2: Supplementary Table 1). Membranes were incubated 1 h at RT with agitation in the corresponding secondary antibody solutions (goat anti-mouse 800 and goat anti-rabbit 680 diluted 1:5000) and revealed using Licor Odyssey Clx. Intensity quantification was performed on ImageJ and each pTau signal was normalized to D5 total tau signal for each sample. For each time-point pTau/D5 ratios were normalized to PBS injected animals. AD brain and TauKO mouse brain homogenates were used as technical positive and negative controls respectively.

Immunohistochemistry

Free-floating 40 µm-thick coronal sections were washed in 0.2% Triton X-100 PBS, incubated 30 min in 0.3% H_2O_2 PBS. After washing in 0.2% Triton X-100 PBS, sections were blocked in 4.5% normal goat serum (Vector Laboratories) in 0.2% Triton X-100 PBS for 1 h then incubated in primary antibody solution in blocking solution at 4 °C overnight (Additional File 2: Supplementary Table 1). The next day, sections were washed in 0.2% Triton X-100 PBS and incubated in secondary antibody solution in blocking solution for 1 h before amplification of the signal by incubation in Vectastain ABC kit (1:400, Vector Laboratories) for 1 h. After wash in 0.2% Triton X-100 PBS, sections were incubated 1 min in DAB (Vector Laboratories) then mounted on Superfrost Plus slides, dehydrated in increasing concentration of ethanol/xylene and coverslipped with Eukitt (Sigma-Aldrich).

Immunofluorescence and thioflavin-S staining

Free-floating 40 µm-thick coronal sections were washed in PBS, blocked with 4.5% normal goat serum (Vector Laboratories) in 0.2% Triton X-100 PBS for 1 h then incubated in primary antibody solution in blocking solution at 4 °C overnight (Additional File 2: Supplementary Table

1). The next day, sections were washed in PBS and incubated in secondary antibody solution in blocking solution for 1 h before being mounted on Superfrost Plus slides and coverslipped with DAPI-containing Fluoromount-G (0100−20, Southern Biotech). When needed, thioflavin-S (ThioS) staining was performed prior to coverslipping by quickly rinsing the dried sections in PBS and incubating in 0.05% Thioflavin-S (ThioS, T1892-25G, Sigma-Aldrich) in 50% ethanol for 8 min in the dark. Sections were then briefly rinsed in 80% ethanol and transferred to dH_2O for 5 min prior to coverslipping.

Image analysis

Immunohistochemistry and immunofluorescence images were acquired at 20x using a NanoZoomer (Hamamatsu) or VS120 (Olympus) slide scanner, respectively. Manual segmentation of the different brain regions and thresholding of each channel was performed on sections spanning the entire hippocampus using QuPath software. DAB-positive, and ThioS-positive cells were manually counted using QuPath cell counter plugin on sections spanning the entire hippocampus. For Iba1-positive rod-microglia quantification, images were taken using the 40x objective on a FV3000 confocal microscope (Olympus). For each animal, quantification was averaged from three fields of view (30 z-stacks, 0.5 µm interval) in the *stratum radiatum* of the dorsal CA1 on 3 sections at 400 µm interval surrounding the injection site. For each field of view, Iba1-positive microglia (average of 24 per field of view across all time-points) were manually segmented using ImageJ. The same Iba1 threshold was applied to each individual cell, the minimum and maximum Feret diameter measured, and the aspect ratio (AR = max Feret/min Feret) calculated. Iba1-positive cells were considered rod-like when they had an AR > 1.6, determined by the average median AR + 2SD (standard deviation) of all PBS-injected animals (6 time-points, $n = 5$/time-point). For each animal, the percentage of Iba1-positive rod-microglia per total Iba1-positive cells was calculated. All quantifications were performed blinded to the injection groups. Representative fluorescent images were acquired on a FV3000 confocal microscope (Olympus).

Statistical analysis

Statistical analyses were performed using GraphPad Prism software. The normality of the distribution and homoscedasticity were checked prior to analysis. For tau immunostainings and dotblot quantifications, t-tests between AD HMW tau and AD SARK tau-injected groups were performed. We used one-way ANOVA to compare all three injection groups. For comparisons over time, two-way ANOVA statistical analysis were performed with Injection group and Time as variables followed by uncorrected Fisher's Least Significant Difference (LSD) multiple comparison as recommended by the software. Data are represented as mean and standard error of mean (mean ± SEM). Outliers identified by GraphPad Prism software 'Identify outlier' plug-in (ROUT Q = 5%) were removed from the analysis.

Results

Differential tau pathology rate of progression and spatial distribution according to the nature of the tau seed

To better understand the chronology of tau seeding, we monitored tau pathology development in an intracerebral injection model which allows us to target a brain region of interest and to control for the start time as well as the nature and amount of potentially pathogenic tau seed preparations. We compared the biological outcomes of AD-derived HMW and AD-derived SARK tau seeds in the dorsal hippocampus of adult human tau-expressing mice (hTau) at 6 different time-points after injection (Additional File 1: Supplementary Fig. 1a). Previous studies showed that hTau mice develop spontaneous tau hyperphosphorylation by 6 months and tau aggregates by 13 months of age [3, 5]. We used hyperphosphorylated tau immunostaining (AT8) at the injection site in the dorsal hippocampus as a readout of induced tau pathology in our injected animals. As expected, no AT8-positive pathology is observed in PBS-injected hTau animals at any time-point up to 3 months post-injection corresponding to 6 months of age (Fig. 1a). In AD HMW and AD SARK tau-injected hTau mice, diffuse AT8 staining restricted to the *corpus callosum* and the injection site along the needle track is observed 1 day after injection (Fig. 1a) reflecting the extracellular injected material (Additional File 1: Supplementary Fig. 1b), but no AT8-positive cell somas are present at any time-point in any brain region including the injection site (dorsal hippocampus) between 1 day and 1 month after injection.

We quantified the number of AT8-positive cells in 10 different brain regions connected to the dorsal hippocampus (injection site) including brain regions of the Papez circuit relevant for AD (mammillary bodies, anterior nuclei of the thalamus, cingulate, entorhinal cortex). While both AD HMW tau and AD SARK tau-injected animals start developing tau pathology 1 month after injection with similar local loads at the injection site, the distribution of AT8-positive cells across brain regions differs. In fact, AD HMW tau-injected animals exhibit prominent tau pathology in the cingulate, subiculum and peri-/entorhinal cortex compared to AD SARK tau-injected mice (Fig. 1b-c). The hippocampus is mainly connected to the perirhinal cortex layer V [1, 59] where most of the AT8-positive neurons of that anatomical area are observed. Interestingly, 3 months after injection of AD HMW tau AT8 pathology starts appearing in the mammillary bodies (Additional File 1: Supplementary

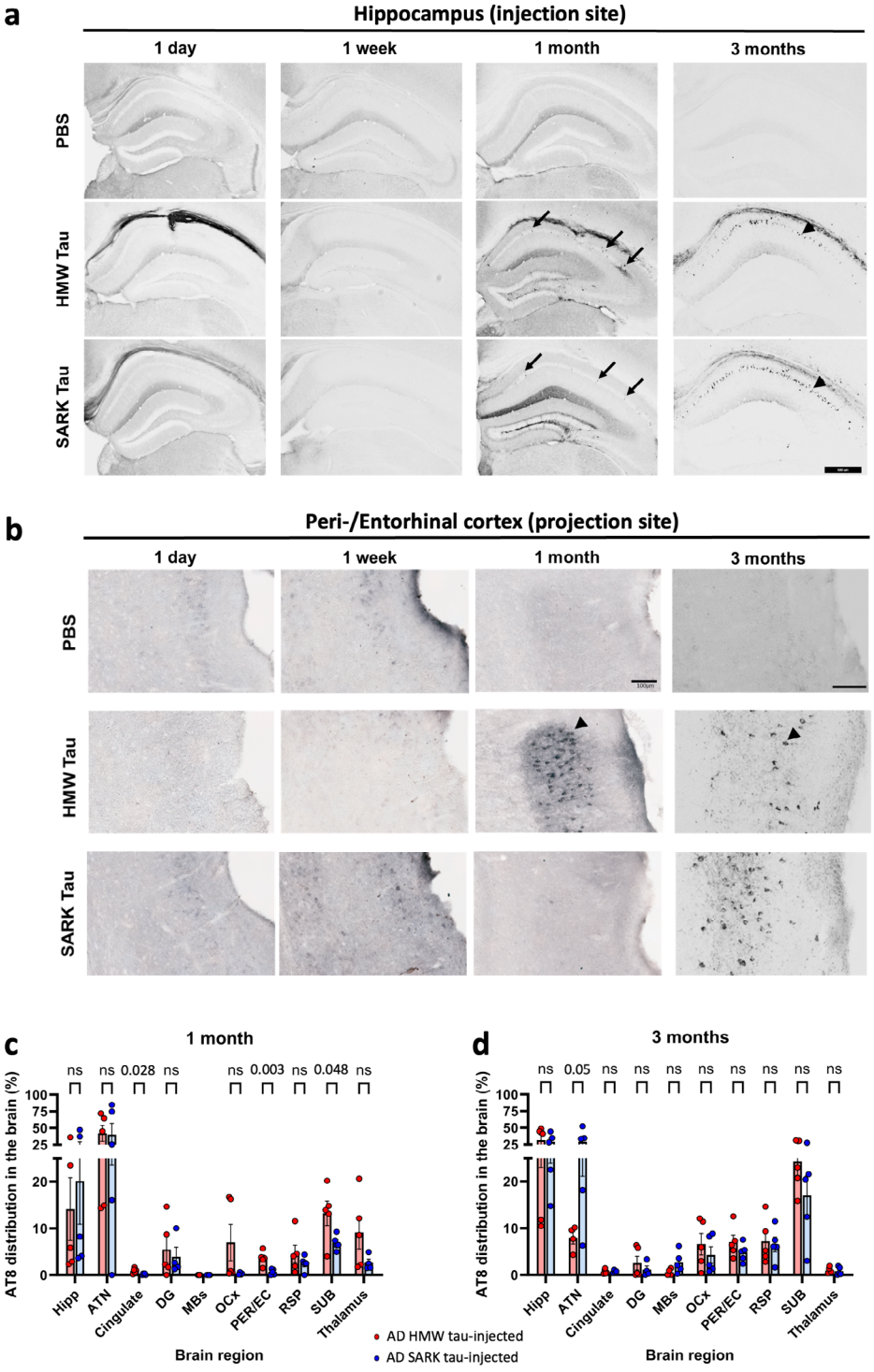

Fig. 1 PBS extractable AD HMW and insoluble AD SARK tau seeds have different pathology distribution patterns over time. **(a)** Representative images of AT8-positive immunostaining at 1 day, 1 week, 1 month, and 3 months after injection in PBS, AD HMW Tau- and AD SARK Tau-injected hTau mice. Sparse AT8-positive cells (arrows) and extensive AT8 tau pathology (arrowheads) are observed in both tau-injected groups 1 and 3 months after injection, respectively. Scale bar = 500 µm. **(b)** Representative images of AT8-positive immunostaining (arrowheads) in the peri-/entorhinal cortex at 1 day, 1 week, 1 month, and 3 months after injection in PBS, AD HMW Tau- and AD SARK Tau-injected hTau mice. Scale bars = 100 µm. **c-d**. Distribution (%) of AT8 pathology across brain regions 1 month and 3 months after injection between AD HMW and AD SARK tau-injected animals. Data represented as mean ± SEM, *n* = 4–6/group, individual t-test for each brain region. HIPP = hippocampus, ATN = anterior thalamus nuclei, DG = dentate gyrus, MBs = mamillary bodies, OCx = hippocampus overlaying cortex (motor and somatosensory), PER/ENT = peri-/entorhinal cortex, RSP = retro-splenial cortex, SUB = subiculum

Fig. 2b) reflecting continuous propagation to anatomically connected regions through the Papez circuit. While very little AT8 pathology was seen in AD SARK tau-injected animals in the peri-/entorhinal cortex 1 month after injection (2 out of 5 animals), AT8 pathology is thoroughly present 3 months after injection in both the peri-/entorhinal cortex and the mammillary body. This suggests that the propagation pathways between AD HMW and AD SARK tau injections are the same, but the kinetics differ. We also observe increased AT8 tau pathology in the perirhinal layer V and entorhinal layer II in both AD tau-injected groups suggesting anterograde and retrograde propagation, respectively. In addition, the presence of tau pathology is nearly significantly higher in the anterior thalamic nuclei (ATN) of AD SARK tau-injected animals compared to AD HMW tau-injected ones (Fig. 1d).

All tau pathology-positive brain regions are primarily or secondarily, via the subiculum, connected to the dorsal CA1 injection site [12, 18, 26, 31, 42, 52, 59], suggesting that, in this model, we indeed observe propagation along neural systems rather than diffusion from the injection site. These data suggest that AD HMW and AD SARK tau seeds extracted from the same AD brain have different pathology kinetics and propagation routes with faster spreading and/or higher vulnerability to AD HMW tau seeds. However, 60% of the AD HMW tau-injected animals present predominant perirhinal layer V AT8 pathology while 60% of the AD SARK tau-injected animals present predominantly entorhinal layer II pathology, arguing in favor of differential neuronal vulnerability to the 2 tau preparations.

To evaluate whether tau itself was responsible for the effects of AD HMW tau and AD SARK tau in the biological outcomes observed in injected hTau mice, we immunodepleted total tau from each AD-derived sample using HT7 anti-tau antibody (Additional File 1: Supplementary Fig. 3a-b) before injecting into the hippocampus of a subset of hTau mice ($n=3$/group). Animals injected with tau-immunodepleted material do not exhibit any AT8 tau pathology in any brain region (Additional File 1: Supplementary Fig. 3c) 1 month after injection. Similarly, tau pathology does not develop after injection into Tau KO mice lacking endogenous tau confirming the templated seeding action of the injected AD-derived tau seeds (Additional File 1: Supplementary Fig. 4a).

Tau seeds characteristics are maintained after in vivo amplification

In the templated misfolding hypothesis, tau may be able to recruit and compromise naïve tau, passing on its own characteristics [54]. Here, in an in vivo amplification model, we used HMW and SARK tau as two distinct tau seeds extracted from the AD brain upon their differential extraction conditions, using PBS and sarkosyl solutions, respectively. Total tau immuno-EM reveals that tau is non-fibrillar in the HMW preparation but is present in both non-fibrillar and fibrillar form in the SARK preparation (Additional File 1: Supplementary Fig. 1d), as previously reported [44, 48]. We applied similar extraction methods to isolate and assess the presence of PBS-extractable and sarkosyl-insoluble bioactive tau seeds from mouse brain homogenates at each time-point after injection (Additional File 1: Supplementary Fig. 2a). PBS-injected hTau mice do not exhibit bioactivity at any time-point demonstrating that hTau mice do not produce endogenous bioactive tau up to 6 months of age.

Curiously, 1 day after injection PBS extractable tau seeds are not only present in the hippocampus of HMW tau-injected animals but also in SARK tau-injected ones, which may result from the association of oligomeric species with native fibrils derived from the AD brains, or from the sonication of SARK tau and the production of more soluble oligomers [32], steps recommended in the literature prior to use [36, 51] (Additional File 1: Supplementary Fig. 1c), or the processing of the fibrils by the murine cells. The bioactivity in the PBS extract of the recipient mice is completely abolished by 2.5 weeks after injection in both tau-injected groups, but it decreases faster in the AD SARK tau-injected animals than in the AD HMW tau-injected animals (Fig. 2a, Two-way ANOVA and uncorrected Fisher's LSD: 3-days HMW vs. 3-days SARK, $p=0.00349$), suggesting distinct clearance kinetics. These observations are in accordance with the histology data where no pathological tau is detected within this time frame (Fig. 1).

Starting from 2.5 weeks post-injection both AD HMW and SARK-injected hTau mice present increasing bioactive PBS extractable tau species in the hippocampus with a faster amplification rate in the AD SARK tau-injected animals (Fig. 2a Two-way ANOVA and uncorrected Fisher's LSD: 1-month HMW vs. 1-month SARK, $p=0.9011$; 3-months HMW vs. 3-months SARK, $p=0.0066$). In contrast, only AD SARK-injected hTau mice contain and amplify bioactive sarkosyl-insoluble tau species locally in the hippocampus (Fig. 2b, Two-way ANOVA and uncorrected Fisher's LSD: 1-day HMW vs. 1-day SARK, $p=0.0149$; 3-months HMW vs. 3-months SARK, $p<0.0001$). Likewise, both PBS-extractable and sarkosyl-insoluble tau seeds are amplified in the AD SARK tau-injected animals in the synaptically connected entorhinal cortex over time (Fig. 2c-d). These data therefore suggest that, within 3 months after injection into hTau mice, AD HMW tau amplifies and propagates only PBS-extractable tau species, while the injection of sonicated AD SARK tau can spread and produce both bioactive PBS-extractable and sarkosyl-insoluble tau species, replicating the initial injected tau seeds observed 1 day after injection.

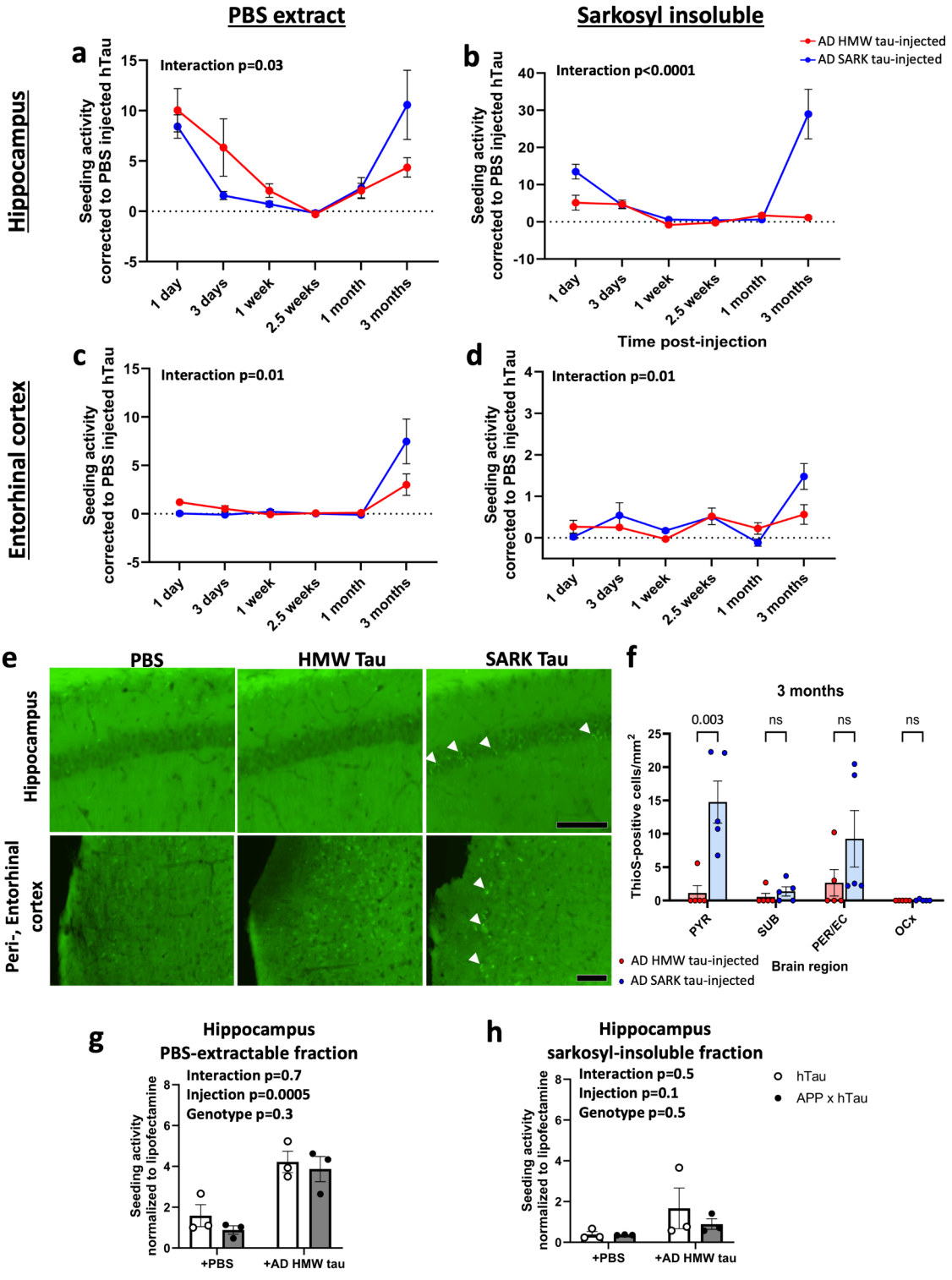

Fig. 2 Tau seeds' characteristics are maintained after in vivo amplification. **a-d.** Quantification of seeding activity over time in PBS and sarkosyl extracts of hippocampal and entorhinal cortex homogenates from injected hTau mice. At each time point, seeding activity was corrected to the corresponding PBS-injected group. The graph shows the average of 3 independent seeding assay. Data represented as mean ± SEM, *n* = 4–6/group, Two-way ANOVA. **e.** Representative images of ThioS-positive staining (arrowheads) at 3 months after injection in PBS, AD HMW Tau- and AD SARK Tau-injected hTau mice. Scale bars = 100 µm. **f.** Quantification of the ThioS-positive cells density in different brain regions. Data represented as mean ± SEM, *n* = 5/group, individual t-test for each brain region. PYR = hippocampal pyramidal layer, SUB = subiculum, PER/ENT = peri-/entorhinal cortex, OCx = hippocampus overlaying cortex (motor and somatosensory). **g-h.** Quantification of seeding activity in PBS and sarkosyl extracts of hippocampal homogenates from injected hTau and APPxhTau mice. The graph shows the average of 3 independent seeding assay. Data represented as mean ± SEM, *n* = 3/group, Two-way ANOVA

To further confirm that the type of tau pathology depends on the nature of the initial tau preparation, we evaluated mature aggregates by quantifying the number of ThioS-positive cells across brain regions. Corroborating our findings, ThioS-positive mature aggregates are present only in the AD SARK tau-injected animals (Fig. 2e-f), starting 3 months after injection together with the appearance of sarkosyl-insoluble tau seeds. In addition, while similar amounts of total tau are present in the recipient mouse PBS extracts (Additional File 1: Supplementary Fig. 5a-b), quantification of tau in the sarkosyl-insoluble fractions by dotblot reveals the increasing presence of sarkosyl-insoluble tau over time in the AD SARK tau-injected animals (Additional File 1: Supplementary Fig. 5c-d). As expected, bioactive tau seeds do not form when tau is immunodepleted from the injected AD tau samples (Additional File 1: Supplementary Fig. 3d) or when endogenous tau is not present as shown by the injection into Tau KO mice (Additional File 1: Supplementary Fig. 4b-e).

We next investigated whether the presence of mutated APP and PS1 would induce the production of sarkosyl-insoluble tau species in an additional batch of hTau mice and hTau mice crossed with the well characterized APP/PS1 mice (APPxhTau). Three months after injection of AD HMW tau or PBS, the hippocampi and cortices were dissected. Both PBS extractable and sarkosyl-insoluble proteins were extracted, and their bioactivity was tested on the in vitro seeding assay. Three months after injection of PBS (corresponding to 6 months of age), neither hTau nor APPxhTau mice display endogenous bioactive tau. While the injection of AD HMW tau results in increased bioactive PBS extractable tau species, the genotype of the recipient mouse does not seem to affect the said amount of bioactivity (Fig. 2g). The presence of APP does not seem to induce the conversion of the amplified PBS-extractable tau seeds into sarkosyl-insoluble seeds as no bioactive sarkosyl-insoluble tau was detected by seeding assay (Fig. 2h). Therefore, the presence of amyloid does not appear to modify the nature of AD HMW tau-induced seeds.

Tau phosphorylation profiles vary over time and with the stage of tau pathology

We show, in vivo, that newly formed tau seeds mimic the characteristics of the initial exogenous AD brain-derived seeds. While sarkosyl-insoluble tau seeds are produced uniquely after the exposure of cells to sarkosyl-insoluble AD SARK tau, PBS-extractable tau seeds are formed after injection of either AD HMW or AD SARK tau. We thus wondered whether these in vivo amplified PBS-extractable seeds were the same in both tau-injected groups. We used denaturing dotblots to screen for various pTau epitopes that we chose based on recently published mass spectrometry data comparing phosphorylation frequencies between AD HMW and AD SARK tau samples [44]. This method only allows the observation of global changes in the whole pool of tau protein. At the injection site in the hippocampus, pTau profiles are already different between tau-injected groups with AD HMW tau-injected animals displaying more tau phosphorylated at S262 (pS262) than AD SARK tau ones (Fig. 3a). This difference is then abolished until 2.5 weeks post-injection, in accordance with decreased bioactivity and the absence of histopathological changes. Interestingly, tau phosphorylation at S396 (pS396) and S195 (Tau1 measures dephosphorylated S195) are increased in the hippocampus of AD SARK tau-injected mice compared to AD HMW tau-injected ones at 2.5 weeks post-injection just before the appearance of tau deposits. These differences are not observed anymore at 1- and 3 months post-injection when both injection groups present similar levels of AT8 tau pathology. Similarly, tau phosphorylation at S396 and S195 is increased in the entorhinal cortex of AD SARK tau-injected animals, at 1-month post-injection, the last time-point preceding AT8 tau deposits in that brain region in those animals (Fig. 3b). These observations suggest that (i) phosphorylation profiles vary over time, (ii) AD HMW and AD SARK-induced PBS-extractable tau seeds are different, and (iii) phosphorylation at S396 and S195 precede and thus may predict AD SARK tau-induced tau deposition.

At 3 months post-injection, AD SARK tau-induced PBS-extractable seeds become more bioactive than AD HMW tau-induced ones, together with the appearance of ThioS-positive mature aggregates and sarkosyl-insoluble tau seeds (Fig. 2). Curiously, it is also the time when AD SARK tau-injected animals have more PBS-extractable and sarkosyl-insoluble tau phosphorylated at T217 (pT217) in the hippocampus (Fig. 3a and c) and the entorhinal cortex (Fig. 3b and d), suggesting phosphorylation at T217 may correlate with AD SARK tau-induced tau pathology.

Microglial response varies over time and with the nature of the tau seeds

Glial reactivity is a major pathological hallmark for AD [58] and has been reported in the propagation of tau pathology [2, 8]. We compared the area covered by GFAP-positive astrocytes (Additional File 1: Supplementary Fig. 6a) and Iba1-positive microglia (Additional File 1: Supplementary Fig. 6b) at the injection site in the hippocampus 2.5 weeks, 1 month and 3 months after injection when tau pathology is absent, starts and amplifies, respectively. Data show no difference between injection groups at any analyzed time point. However, the morphology of Iba1-positive microglial cells seems to vary over time with the appearance of rod-like microglia in

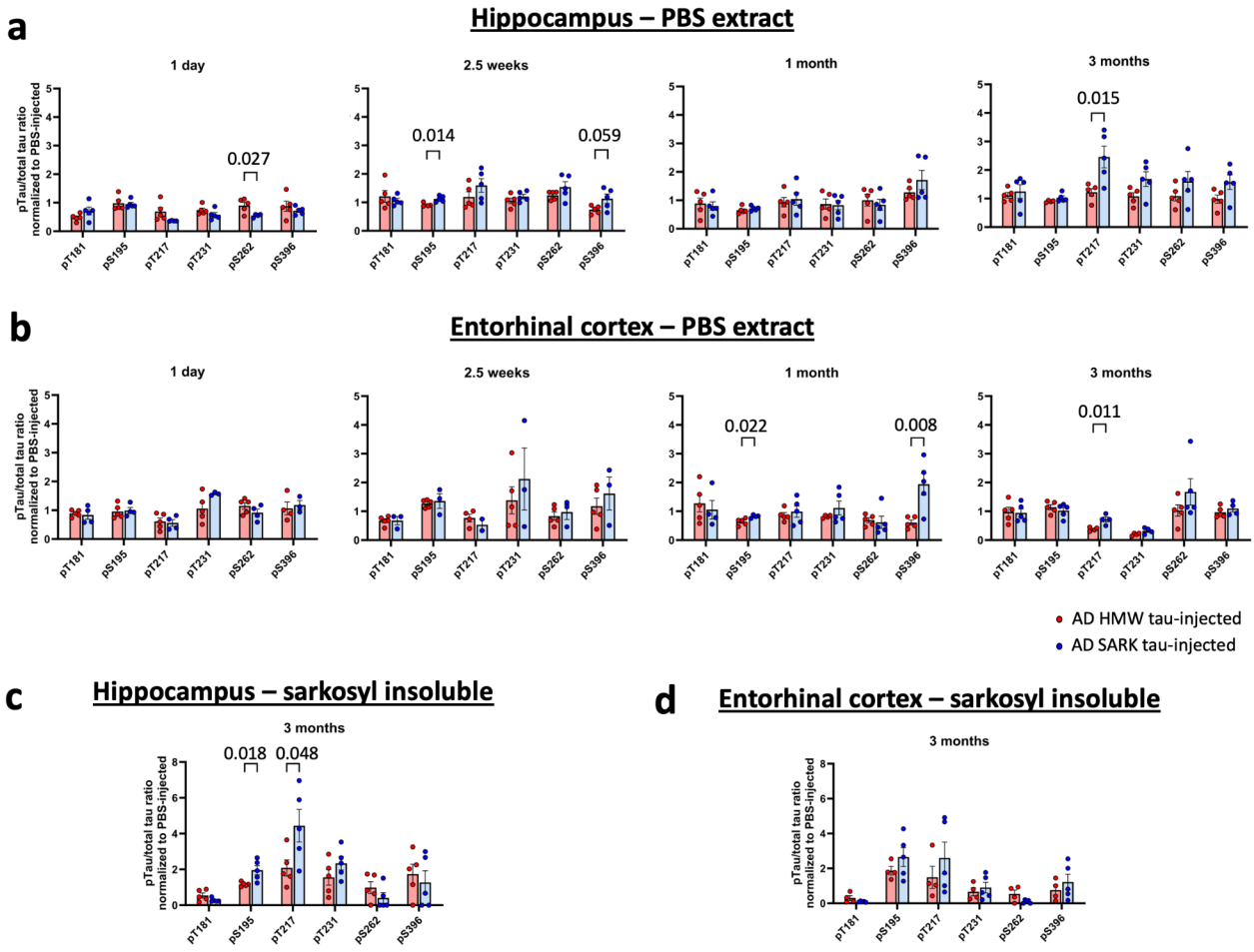

Fig. 3 Endogenous Tau phosphorylation profiles differ according to tau pathology stage. **(a)** Quantification of various pTau epitopes (normalized to total tau) over time in PBS extracts of hippocampal homogenates from injected hTau mice. **(b)** Quantification of various pTau epitopes (normalized to total tau) over time in PBS extracts of entorhinal cortex homogenates from injected hTau mice. **(c)** Quantification of various pTau epitopes (normalized to total tau) 3 months after injection in sarkosyl extracts of hippocampal homogenates from injected hTau mice. **(d)** Quantification of various pTau epitopes (normalized to total tau) 3 months after injection in sarkosyl extracts of entorhinal cortex homogenates from injected hTau mice. At each time point, data was normalized to the corresponding PBS-injected group. Phosphorylation at S195 (pS195) was measured using Tau1 antibody which recognizes dephosphorylated tau S195, and the inverse reported on the graph for visualization purposes. Data represented as mean ± SEM, $n = 4–6$/group, individual t-test for each pTau

the hippocampus of both tau-injected groups (Fig. 4a). Subsequent quantification reveals a differential phenotypic change with a high presence of rod-microglia after AD HMW tau injection at almost every time point with a drop observed 3 months after injection (Fig. 4b). In AD SARK tau-injected animals, the rod-microglia peak happens at 1- and 2.5 weeks post-injection, after the injected material has been cleared from the hippocampus and before the detection of newly formed seeds and tau pathology. These data suggest that Iba1-positive microglia behave differently according to the nature of the initial tau seed. These data are consistent with the hypothesis that rod-microglia are involved in the spread of pathological tau seeds as they are more prominent in the AD HMW tau-injected animals where tau pathology spreads faster than in AD SARK tau-injected animals.

We further focused on the 1 month after injection time-point when, in the hippocampus, the only difference between the two tau-injected groups is the abundance of rod-like microglia. We do not observe differences in atrophy (Additional File 1: Supplementary Fig. 6c) or synapse loss (Additional File 1: Supplementary Fig. 6e). Likewise, no noticeable neuronal loss is observed at 3 months post-injection (Additional File 1: Supplementary Fig. 6d), suggesting neither detrimental nor protective effects on neurons of rod-like microglia in these conditions.

Discussion

AD is characterized by its spatiotemporal progression pattern based on the distribution of protein aggregates across the brain resulting in Thal and Braak disease staging for amyloid β [65] and tau [15], respectively. Cognitive

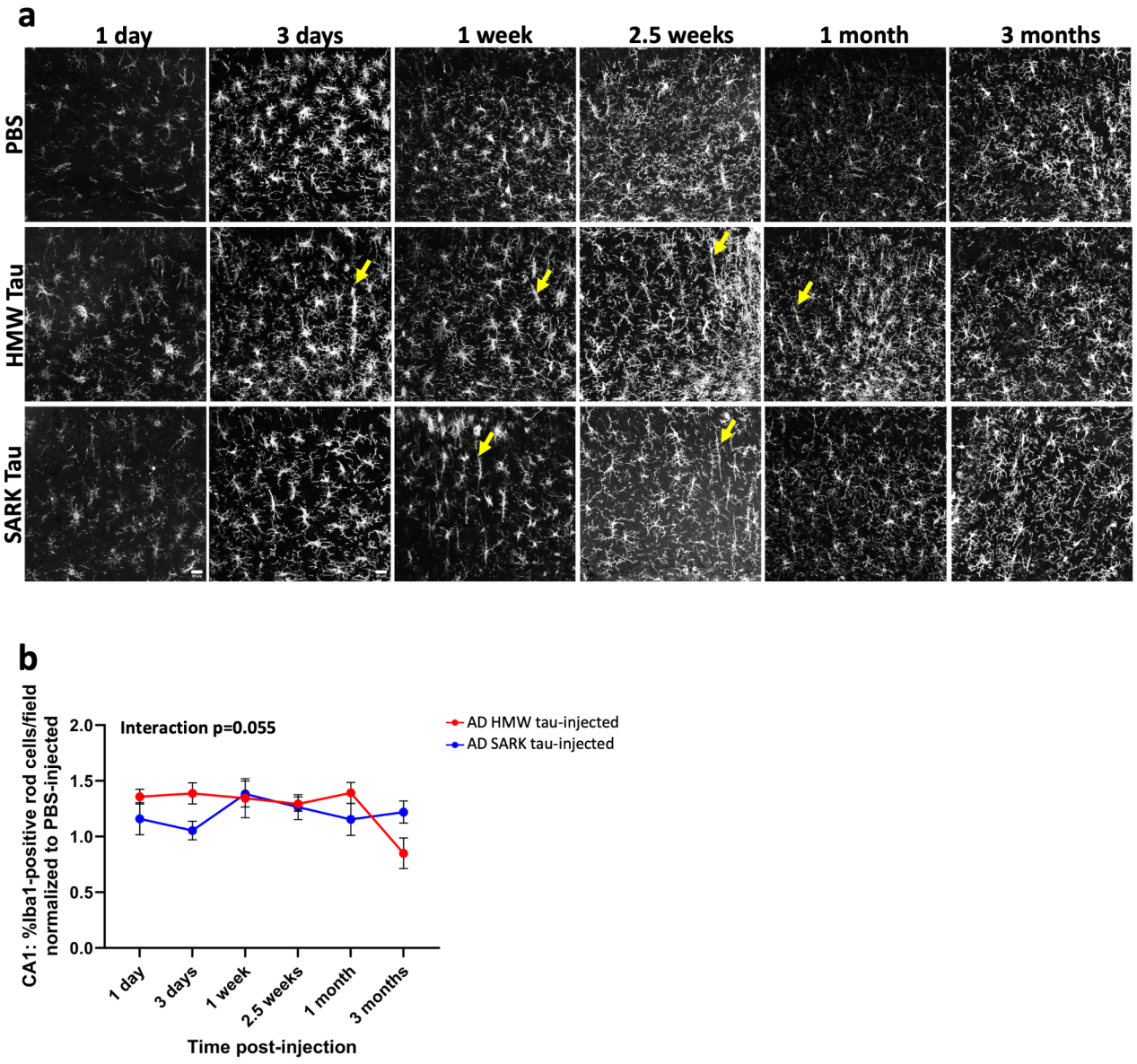

Fig. 4 Microglial phenotype varies over time and with the nature of the exogenous Tau seed. **(a)** Representative images of the morphology of Iba1-positive microglia in the CA1 of the hippocampus of PBS, AD HMW, and AD SARK tau-injected mice over time. Rod-like microglia are observed at different time-points (yellow arrows). **(b)** Quantification of the percentage of rod-like Iba1-positive cells normalized to PBS-injected animals at each time point. Data represented as mean ± SEM, $n = 4–6$/group, Two-way ANOVA

decline is tightly correlated with Braak stage as the fibrillar tangles appear to spread across limbic and association areas [7, 33]. However, recent biochemical evidence shows that both fibrillar and non-fibrillar tau species may impact progression [27], suggesting that multiple seed-competent tau species can co-exist in the AD brain [48]. In the present study, we compared PBS-extractable HMW tau (AD HMW tau) and sarkosyl-insoluble tau (AD SARK tau), two distinct and well-characterized tau seed-competent preparations present in the AD brain, to better understand the contribution of each species to the spatiotemporal kinetics of tau pathology. We conclude that AD HMW tau and AD SARK tau could be considered two distinct tau seeds as (i) tau pathology develops faster in connected brain regions in the presence of AD HMW tau, (ii) the triggered tau pathology recapitulates the properties of the original tau seeds (Fig. 5).

Tau pathology propagation along neural systems has been long demonstrated in vivo, where the injection of recombinant [26, 34, 40, 41, 53] or brain-derived tau [23, 36, 45, 48] is followed by the appearance of tau aggregates in the contralateral hemisphere and/or connected brain regions such as the entorhinal cortex. Curiously, the amount of induced tau pathology and the timeframe for

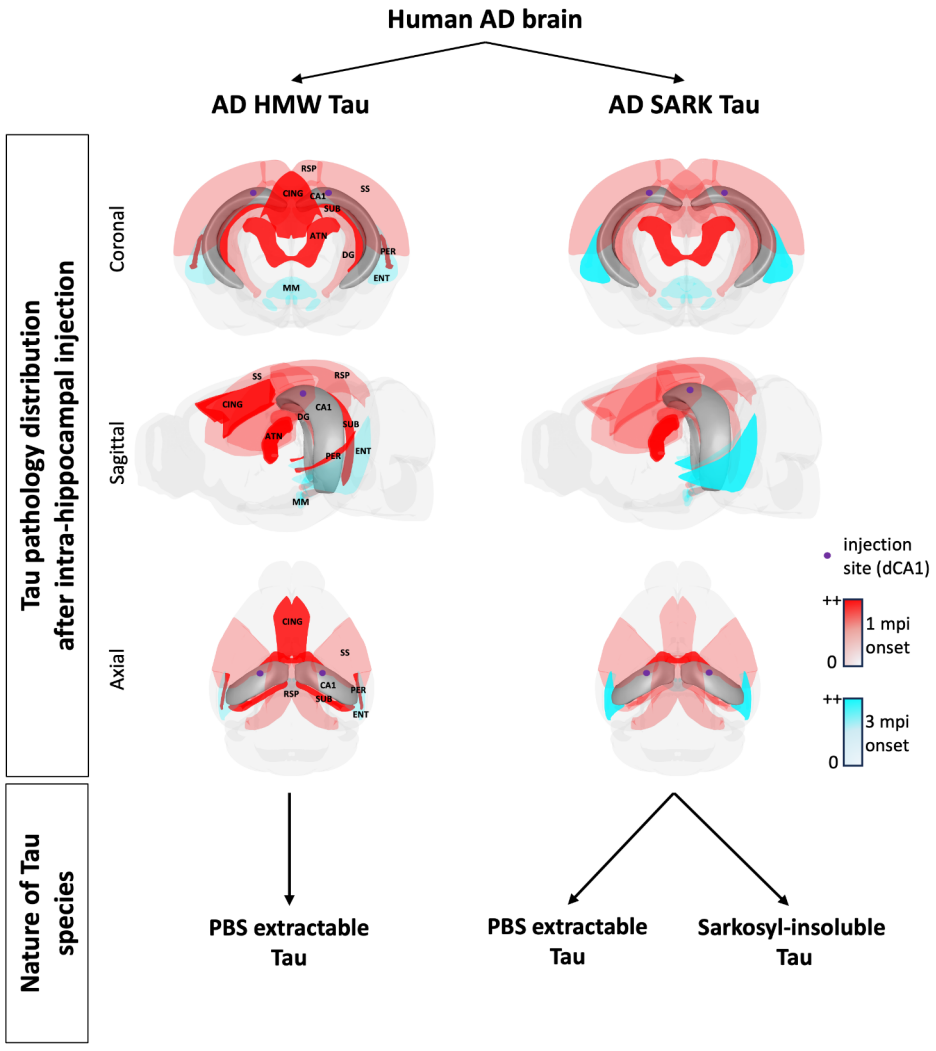

Fig. 5 Human AD brain contains multiple distinct tau pathologies. The human AD brain contains various tau species that can be differentially extracted based on their solubility: PBS-extractable AD HMW tau and sarkosyl-insoluble AD SARK tau. In vivo in hTau mice, both species start inducing pathology 1 month after injection (red colors), but the spatial distribution of tau pathology differs across injection groups. Heavier tau loads (bright red vs. light red) are observed in AD HMW tau-injected mice in the subiculum, cingulate, and perirhinal region compared to AD SARK-injected animals. Within 3 months after injection (blue colors), AD SARK tau-injected animals also present tau pathology in the peri-/entorhinal region, and all AD tau-injected mice start getting tau pathology in the mammillary bodies. All tau pathology-bearing brain regions are either directly or indirectly, via the subiculum, connected to the injection site in the dorsal CA1 (purple dot). Importantly, AD HMW tau seeds amplify as PBS-extractable tau species, while AD SARK tau gives rise to sarkosyl-insoluble tau. Considering the definition of prion strains [17], these different observed characteristics suggest that AD HMW tau and AD SARK tau are distinct substrains of AD tau. CA1: CA1 field of the hippocampus, SUB: subiculum, DG: dentate gyrus, SS: somatosensory cortex, CING: cingulate, RSP: retrosplenial cortex, ATN: anterior thalamic nuclei, PER: perirhinal cortex layer V, ENT: entorhinal cortex layer II, MM: mammillary bodies. The images were generated using the Scalable Brain Atlas composer

such aggregation differs among experimental paradigms. These differences in rate of progression have been shown to depend not only on the tau specie itself [28, 43, 46, 48] but also on the genetic background of the mouse used for the experiment [30, 69]. We here confirm that distinct tau species, isolated from the same AD brain, trigger tau pathology in distal areas within different time frames. Our data show that AD HMW tau injection into the dorsal hippocampus promotes AT8-positive tau pathology accumulation in the entorhinal cortex earlier, at 1-month post-injection, compared to AD SARK tau injection. Whether this differential tau pathology distribution across brain regions results from tau seed propagation kinetics per se or differential regional vulnerability to tau pathology (e.g. wolframin-1-expressing neurons [19, 25]) remains uncertain. However, hippocampal connectivity data in the mouse brain shows both a direct and an indirect connection via the subiculum between the dorsal hippocampus and the entorhinal cortex [26, 52]. The absence of neurodegeneration and presence of extensive

tau pathology in both the subiculum and perirhinal cortex of AD HMW tau-injected animals as early as 1-month post-injection compared to AD SARK tau-injected ones argues in favor of initial anterograde propagation of bioactive AD HMW tau seeds [26]. In our model, we further observe tau pathology progression in the Papez circuit and the mammillary bodies in both AD HMW and AD SARK tau injection groups 3 months after injection suggesting continuous antero- and retrograde propagation of newly formed bioactive tau seeds.

AD pathology is also characterized by astrocytic and microglial activation [58]. Such glial changes have been described as preceding tau tangle formation [63], and it has been reported that microglia depletion in tau mouse models halted tau propagation [8, 16] and neurodegeneration [47]. For these reasons, we evaluated astrocytic and microglial activation at each time point but did not observe any difference between injection groups. However, we did observe an increased appearance of rod-like microglia in the tau-injected groups even before the appearance of tau aggregates but with differences in behavior over time between AD HMW and AD SARK tau-injected groups. Similar to what we previously described in injected PS19 mice [48], AD HMW tau-injected animals present more rod-like microglia in the hippocampus at 1 month post-injection paralleling the first observations of tau deposits in the entorhinal cortex. At 3 months post-injection it is in the AD SARK tau-injected group that we observe more rod-like microglia, curiously paralleling again the first detection of tau deposits in the entorhinal cortex in these animals.

In a healthy human brain, the half-life of neuronal tau has been measured to be around 23 days, and about 6 days in iPSC neurons with 4R and phosphorylated tau exhibiting a higher turnover [57], but the half-life of extracellular pathological tau has not yet been assessed. We used tau null TauKO mice and hTau mice that physiologically express all 6 human tau isoforms in a mouse tau null background and do not spontaneously accumulate tau until late ages [4] to evaluate exogenous injected AD HMW and AD SARK tau seeds' clearance and amplification over time. Consistent with previously published work, while we can detect some tau staining by histology at the injection site the day following the injection, within 1 week after injection we do not observe any [38]. In parallel, bioactivity data in recipient TauKO and hTau mice show a progressive decrease in seeding activity at the injection site, suggesting that the injected AD tau seeds have been cleared from the hippocampus within 2 weeks with a half-life of about 3 days for AD HMW tau and of 2 days for AD SARK tau.

Recent mass spectrometry data revealed that AD tau is highly modified by phosphorylation, ubiquitination, and acetylation at various epitopes [70] and these post-translational modifications may contribute to its seeding activity [29, 71]. In addition, the progressive hyperphosphorylation of tau may result from a few initial "master-sites", including T181 (pT181), provoking subsequent multi-site phosphorylation [62]. We thus decided to screen our injected mouse brain homogenates over time for a few phospho-epitopes by denaturing dot-blot, choosing them based on the availability of commercial antibodies and relative frequency on AD HMW or AD SARK tau [44]. At the injection site in the hippocampus, AD HMW tau-injected animals display more tau phosphorylated at S262 (pS262) than AD SARK tau-injected ones. Pseudo-phosphorylation at S262 has been shown to promote the disassembly of tau protein from the microtubules leading to enhanced intracellular tau accumulation [61], suggesting that AD HMW tau seeds may accelerate pathology progression through this pathway. Interestingly, in both the hippocampus and the entorhinal cortex our data show that phosphorylation at S195 (pS195) and S396 (pS396) seem to precede tau deposition in AD SARK tau-injected animals. Moreover, these specific phospho-epitopes are more frequent in sarkosyl-insoluble AD brain extracts [44] suggesting a specific signature triggered by AD SARK tau seeds. Finally, we observe enhanced phosphorylation at T217 (pT217) in AD SARK tau-injected animals only, concomitant to the presence of mature ThioS-positive aggregates and sarkosyl-insoluble tau seeds. Combined with recent findings about pT217 as a biomarker for tau in AD [9, 11], our data suggest that pT217 reflects late-stage tau pathology triggered by AD SARK tau seeds.

By analogy to prion diseases and synucleinopathies [67], the different existing tauopathies (AD, PSP, CBD, etc.) are sometimes considered to represent different strains [14, 22, 43, 50, 56, 60] conventionally defined as having [17]: (i) similar underlying molecules, (ii) different conformations, (iii) different rates of propagation after injection, (iv) the ability to induce templated misfolding that replicates the original conformation, and (v) different patterns of distribution.

Mass spectrometry of PBS-extractable HMW and sarkosyl-insoluble SARK tau demonstrates that they are both highly modified tau species, and the modifications are strikingly similar, although distinct, with SARK tau being much more modified than HMW tau [44, 70]. They are clearly conformationally distinct [48]: SARK PHF have β-pleated sheet conformation [13] whereas HMW tau are likely conformationally flexible, non-β-sheet oligomers as assessed by atomic force microscopy (AFM) [64] and EM [44, 48]. PBS-extractable HMW and fibrillar tau could, in some sense, be considered two different species of AD tau seeds since they share the same underlying tau molecule but have different post-translational modifications, are structurally distinct and have different

properties after injection into a naïve host. However, importantly, their concurrent presence within the same brain would be unexpected for the conventional use of the term "strain". We suggest that one way to think about this nomenclature is if they represent one or more substrains of Alzheimer-related tau species.

Besides distinct spreading kinetics, we show that the amplified tau seeds replicate their respective original material. Indeed, AD HMW tau isolated from PBS extracts triggers solely PBS-extractable bioactive tau species. In contrast, sarkosyl-insoluble bioactive tau species are only detected in mice exposed to AD SARK tau. The additional presence of bioactive PBS extractable species after injection of AD SARK tau does not seem surprising as the sample was sonicated prior to injection, and it has been shown that sonication can produce small bioactive oligomeric tau species [32, 49]. Our data confirm that upon sonication AD SARK tau contains a mix of insoluble and soluble species, both being amplified after injection into hTau mouse brain. Consistent with these data, recent elegant array tomography and immunoelectron microscopy experiments with the oligomer- specific T22 antibody show that, in human tissue, some fibrils appear to be decorated by T22-positive immunopositivity [24]. Moreover, T22-positive nonfibrillar tau was identified in pre- and post-synaptic structures, supporting the idea that this nonfibrillar tau contributed to synaptic spread across neural systems [24].

Some articles have reported enhanced tau pathology [66] and the presence of sarkosyl-insoluble tau species [37, 68] after injection of AD SARK tau seeds into amyloid β mouse models, suggesting that the presence of APP accelerates tau pathology. To test whether AD HMW tau is an "immature" form of AD SARK tau, we injected AD HMW tau into the brain of mice expressing both human tau and APP/PS1 (APPxhTau). Our data show that 3 months after injection, even in the presence of Aβ triggering factors, AD HMW tau-induced bioactive seeds remain PBS extractable. One previous study reported AD brain-derived tau injection into a double human tau and APP transgenic mouse model [55]. In that case, AD SARK tau has been injected and histology shows increased tau pathology, but no biochemical characterization of the amplified tau seeds was detailed. The fact that the presence of APP does not modify the nature of AD HMW tau-induced seeds towards a sarkosyl-insoluble form further suggests that AD HMW is not an immediate precursor of AD SARK tau, at least in the time frames and experimental conditions examined here. In addition, a recent in silico paper reported the possibility for the AD tau core to undergo two parallel oligomerization pathways leading to either amorphous nonfibrillar aggregates or ordered fibrils [20]. These structurally distinct aggregates are reminiscing of the amorphous HMW and fibrillar SARK tau isolated from the AD brain and strengthen our observations of two types of tau in AD pathology. Simulations further show that structural interconversion is unlikely and support our in vivo results on the absence of tau fibrils formation after injection of amorphous AD HMW tau.

Conclusions

Taken together, our data further confirm the existence of, at least, two distinct forms of tau that are each capable of supporting templated misfolding occurrence in the AD brain. PBS-extractable (AD HMW tau) and sarkosyl-insoluble (AD SARK tau) tau seeds can both template endogenous tau and we demonstrate that newly formed seeds reflect the initial properties. Importantly, these differences suggest the co-existence of (at least 2) bioactive tau pathologies within the AD brain. We speculate that there may be an entire spectrum of tau conformers in AD brains. If so, the particular patterns of tau deposition, rate of spread, and hence clinical phenomenon may represent patient-specific differences in these populations of conformers. Further characterization will unravel their specific contribution to disease onset and/or rate and patterns of progression and help select patient-specific biomarkers, potentially critical for understanding tau's contribution to neurodegeneration in AD patients.

Abbreviations

AD	Alzheimer's disease
EM	Electron microscopy
HMW Tau	High Molecular Weight Tau (PBS extractable)
ID	Immunodepleted
IFD	Integrated FRET density
NFT	Neurofibrillary tangle
PHF	Paired helical filament
RT	Room temperature
SARK Tau	Sarkosyl-insoluble Tau (fibrillar)
SEC	Size-exclusion chromatography
v/w	Volume per weight
WB	Western blot

Supplementary Information

The online version contains supplementary material available at https://doi.org/10.1186/s40478-024-01849-1.

Supplementary Material 1

Acknowledgements

We are grateful for Alzheimer's disease patients and the Massachusetts ADRC brain bank for providing the tissue samples. We thank Professor Adriano Aguzzi, University of Zurich, for critical reading of the manuscript. We thank Analiese Fernandes and Simon Dujardin for the breedings of hTau and Tau KO mice. This work was supported by the Rainwater Foundation, the JPB Foundation, P30AG062421 and R01AG059789.

Author contributions

AMG and BTH conceived the study and designed the experiments. AMG, AK, LAW, HB, CG and RP performed experiments and analyzed data. NQ and RP provided critical input on the study. The manuscript was written by AMG and BTH with input from all the authors.

Data availability
All data supporting the findings of this study can be found within the article and its supplementary information or available from the corresponding author upon reasonable request.

Declarations

Disclosure and competing interest
The authors declare that they have no competing interests.

Received: 3 July 2024 / Accepted: 8 August 2024
Published online: 09 September 2024

References

1. Agster KL, Burwell RD (2013) Hippocampal and subicular efferents and afferents of the perirhinal, postrhinal, and entorhinal cortices of the rat. Behav Brain Res 254:50–64. https://doi.org/10.1016/j.bbr.2013.07.005
2. Amro Z, Yool AJ, Collins-Praino LE (2021) The potential role of glial cells in driving the prion-like transcellular propagation of tau in tauopathies. Brain Behav Immun - Health 14:100242. https://doi.org/10.1016/j.bbih.2021.100242
3. Andorfer C, Acker CM, Kress Y, Hof PR, Duff K, Davies P (2005) Cell-cycle reentry and cell death in transgenic mice expressing nonmutant human tau isoforms. J Neurosci off J Soc Neurosci 25:5446–5454. https://doi.org/10.1523/JNEUROSCI.4637-04.2005
4. Andorfer C, Kress Y, Espinoza M, de Silva R, Tucker KL, Barde Y-A, Duff K, Davies P (2003) Hyperphosphorylation and aggregation of tau in mice expressing normal human tau isoforms. J Neurochem 86:582–590. https://doi.org/10.1046/j.1471-4159.2003.01879.x
5. Andorfer C, Kress Y, Espinoza M, Silva RD, Tucker KL, Barde Y-A, Duff K, Davies P (2003) Hyperphosphorylation and aggregation of tau in mice expressing normal human tau isoforms. J Neurochem 86:582–590. https://doi.org/10.1046/j.1471-4159.2003.01879.x
6. Arakhamia T, Lee CE, Carlomagno Y, Duong DM, Kundinger SR, Wang K, Williams D, DeTure M, Dickson DW, Cook CN, Seyfried NT, Petrucelli L, Fitzpatrick AWP (2020) Posttranslational modifications mediate the structural diversity of Tauopathy strains. Cell 180:633–644e12. https://doi.org/10.1016/j.cell.2020.01.027
7. Arriagada PV, Growdon JH, Hedley-Whyte ET, Hyman BT (1992) Neurofibrillary tangles but not senile plaques parallel duration and severity of Alzheimer's disease. Neurology 42:631–639. https://doi.org/10.1212/wnl.42.3.631
8. Asai H, Ikezu S, Tsunoda S, Medalla M, Luebke J, Haydar T, Wolozin B, Butovsky O, Kügler S, Ikezu T (2015) Depletion of microglia and inhibition of exosome synthesis halt tau propagation. Nat Neurosci 18:1584–1593. https://doi.org/10.1038/nn.4132
9. Ashton NJ, Brum WS, Di Molfetta G, Benedet AL, Arslan B, Jonaitis E, Langhough RE, Cody K, Wilson R, Carlsson CM, Vanmechelen E, Montoliu-Gaya L, Lantero-Rodriguez J, Rahmouni N, Tissot C, Stevenson J, Servaes S, Therriault J, Pascoal T, Lleó A, Alcolea D, Fortea J, Rosa-Neto P, Johnson S, Jeromin A, Blennow K, Zetterberg H (2024) Diagnostic Accuracy of a Plasma Phosphorylated Tau 217 Immunoassay for Alzheimer Disease Pathology. JAMA Neurol e235319. https://doi.org/10.1001/jamaneurol.2023.5319
10. Audouard E, Houben S, Masaracchia C, Yilmaz Z, Suain V, Authelet M, De Decker R, Buée L, Boom A, Leroy K, Ando K, Brion J-P (2016) High-molecular-weight paired helical filaments from Alzheimer Brain induces seeding of wild-type mouse tau into an argyrophilic 4R Tau Pathology in vivo. Am J Pathol 186:2709–2722. https://doi.org/10.1016/j.ajpath.2016.06.008
11. Barthélemy NR, Bateman RJ, Hirtz C, Marin P, Becher F, Sato C, Gabelle A, Lehmann S (2020) Cerebrospinal fluid phospho-tau T217 outperforms T181 as a biomarker for the differential diagnosis of Alzheimer's disease and PET amyloid-positive patient identification. Alzheimers Res Ther 12. https://doi.org/10.1186/s13195-020-00596-4
12. Beerens S, Vroman R, Webster JF, Wozny C (2021) Probing subicular inputs to the medial prefrontal cortex. iScience 24:102856. https://doi.org/10.1016/j.isci.2021.102856
13. Berriman J, Serpell LC, Oberg KA, Fink AL, Goedert M, Crowther RA (2003) Tau filaments from human brain and from in vitro assembly of recombinant protein show cross-β structure. Proc Natl Acad Sci 100:9034–9038. https://doi.org/10.1073/pnas.1530287100
14. Boluda S, Iba M, Zhang B, Raible KM, Lee VM-Y, Trojanowski JQ (2015) Differential induction and spread of tau pathology in young PS19 tau transgenic mice following intracerebral injections of pathological tau from Alzheimer's disease or corticobasal degeneration brains. Acta Neuropathol (Berl) 129:221–237. https://doi.org/10.1007/s00401-014-1373-0
15. Braak H, Braak E (1991) Neuropathological stageing of Alzheimer-related changes. Acta Neuropathol (Berl) 82:239–259. https://doi.org/10.1007/BF00308809
16. Bussian TJ, Aziz A, Meyer CF, Swenson BL, van Deursen JM, Baker DJ (2018) Clearance of senescent glial cells prevents tau-dependent pathology and cognitive decline. Nature 562:578. https://doi.org/10.1038/s41586-018-0543-y
17. Carta M, Aguzzi A (2022) Molecular foundations of prion strain diversity. Curr Opin Neurobiol 72:22–31. https://doi.org/10.1016/j.conb.2021.07.010
18. CENQUIZCA LA, SWANSON LW (2007) Spatial Organization of direct hippocampal field CA1 axonal projections to the Rest of the cerebral cortex. Brain Res Rev 56:1–26. https://doi.org/10.1016/j.brainresrev.2007.05.002
19. Chen S, Acosta D, Li L, Liang J, Chang Y, Wang C, Fitzgerald J, Morrison C, Goulbourne CN, Nakano Y, Villegas NCH, Venkataraman L, Brown C, Serrano GE, Bell E, Wemlinger T, Wu M, Kokiko-Cochran ON, Popovich P, Flowers XE, Honig LS, Vonsattel JP, Scharre DW, Beach TG, Ma Q, Kuret J, Kõks S, Urano F, Duff KE, Fu H (2022) Wolframin is a novel regulator of tau pathology and neurodegeneration. Acta Neuropathol (Berl) 143:547–569. https://doi.org/10.1007/s00401-022-02417-4
20. Chen X, Chen M, Schafer NP, Wolynes PG (2020) Exploring the interplay between fibrillization and amorphous aggregation channels on the energy landscapes of tau repeat isoforms. Proc Natl Acad Sci 117:4125–4130. https://doi.org/10.1073/pnas.1921702117
21. Chung DC, Roemer S, Petrucelli L, Dickson DW (2021) Cellular and pathological heterogeneity of primary tauopathies. Mol Neurodegener 16:57. https://doi.org/10.1186/s13024-021-00476-x
22. Clavaguera F, Akatsu H, Fraser G, Crowther RA, Frank S, Hench J, Probst A, Winkler DT, Reichwald J, Staufenbiel M, Ghetti B, Goedert M, Tolnay M (2013) Brain homogenates from human tauopathies induce tau inclusions in mouse brain. Proc Natl Acad Sci 110:9535–9540. https://doi.org/10.1073/pnas.1301175110
23. Clavaguera F, Bolmont T, Crowther RA, Abramowski D, Frank S, Probst A, Fraser G, Stalder AK, Beibel M, Staufenbiel M, Jucker M, Goedert M, Tolnay M (2009) Transmission and spreading of tauopathy in transgenic mouse brain. Nat Cell Biol 11:909–913. https://doi.org/10.1038/ncb1901
24. Colom-Cadena M, Davies C, Sirisi S, Lee J-E, Simzer EM, Tzioras M, Querol-Vilaseca M, Sánchez-Aced É, Chang YY, Holt K, McGeachan RI, Rose J, Tulloch J, Wilkins L, Smith C, Andrian T, Belbin O, Pujals S, Horrocks MH, Lleó A, Spires-Jones TL (2023) Synaptic oligomeric tau in Alzheimer's disease - A potential culprit in the spread of tau pathology through the brain. Neuron 111:2170–2183e6. https://doi.org/10.1016/j.neuron.2023.04.020
25. Delpech J-C, Pathak D, Varghese M, Kalavai SV, Hays EC, Hof PR, Johnson WE, Ikezu S, Medalla M, Luebke JI, Ikezu T (2021) Wolframin-1-expressing neurons in the entorhinal cortex propagate tau to CA1 neurons and impair hippocampal memory in mice. Sci Transl Med 13:eabe8455. https://doi.org/10.1126/scitranslmed.abe8455
26. Detrez JR, Maurin H, Van Kolen K, Willems R, Colombelli J, Lechat B, Roucourt B, Van Leuven F, Baatout S, Larsen P, Nuydens R, Timmermans J-P, De Vos WH (2019) Regional vulnerability and spreading of hyperphosphorylated tau in seeded mouse brain. Neurobiol Dis 127:398–409. https://doi.org/10.1016/j.nbd.2019.03.010
27. Doody RS, Massman P, Dunn JK (2001) A method for estimating Progression Rates in Alzheimer Disease. Arch Neurol 58:449–454. https://doi.org/10.1001/archneur.58.3.449
28. Dujardin S, Bégard S, Caillierez R, Lachaud C, Carrier S, Lieger S, Gonzalez JA, Deramecourt V, Déglon N, Maurage C-A, Frosch MP, Hyman BT, Colin M, Buée L (2018) Different tau species lead to heterogeneous tau pathology propagation and misfolding. Acta Neuropathol Commun 6:132. https://doi.org/10.1186/s40478-018-0637-7
29. Dujardin S, Commins C, Lathuiliere A, Beerepoot P, Fernandes AR, Kamath TV, De Los Santos MB, Klickstein N, Corjuc DL, Corjuc BT, Dooley PM, Viode A, Oakley DH, Moore BD, Mullin K, Jean-Gilles D, Clark R, Atchison K, Moore R, Chibnik LB, Tanzi RE, Frosch MP, Serrano-Pozo A, Elwood F, Steen JA, Kennedy ME, Hyman BT (2020) Tau molecular diversity contributes to clinical heterogeneity in Alzheimer's disease. Nat Med 26:1256–1263. https://doi.org/10.1038/s41591-020-0938-9
30. Dujardin S, Fernandes A, Bannon R, Commins C, De Los Santos M, Kamath TV, Hayashi M, Hyman BT (2022) Tau propagation is dependent on the

genetic background of mouse strains. Brain Commun 4:fcac048. https://doi.org/10.1093/braincomms/fcac048
31. Fanselow MS, Dong H-W (2010) Are the dorsal and ventral Hippocampus functionally. Distinct Structures? Neuron 65:7–19. https://doi.org/10.1016/j.neuron.2009.11.031
32. Ghag G, Bhatt N, Cantu DV, Guerrero-Munoz MJ, Ellsworth A, Sengupta U, Kayed R (2018) Soluble tau aggregates, not large fibrils, are the toxic species that display seeding and cross-seeding behavior. Protein Sci Publ Protein Soc 27:1901–1909. https://doi.org/10.1002/pro.3499
33. Giannakopoulos P, Herrmann FR, Bussière T, Bouras C, Kövari E, Perl DP, Morrison JH, Gold G, Hof PR (2003) Tangle and neuron numbers, but not amyloid load, predict cognitive status in Alzheimer's disease. Neurology 60:1495–1500. https://doi.org/10.1212/01.wnl.0000063311.58879.01
34. Gibbons GS, Banks RA, Kim B, Xu H, Changolkar L, Leight SN, Riddle DM, Li C, Gathagan RJ, Brown HJ, Zhang B, Trojanowski JQ, Lee VM-Y (2017) GFP-Mutant Human Tau Transgenic Mice Develop Tauopathy Following CNS Injections of Alzheimer's brain-derived pathological tau or synthetic mutant human tau fibrils. J Neurosci 37:11485–11494. https://doi.org/10.1523/JNEUROSCI.2393-17.2017
35. Goedert M, Spillantini MG, Cairns NJ, Crowther RA (1992) Tau proteins of alzheimer paired helical filaments: abnormal phosphorylation of all six brain isoforms. Neuron 8:159–168. https://doi.org/10.1016/0896-6273(92)90117-V
36. Guo JL, Narasimhan S, Changolkar L, He Z, Stieber A, Zhang B, Gathagan RJ, Iba M, McBride JD, Trojanowski JQ, Lee VMY (2016) Unique pathological tau conformers from Alzheimer's brains transmit tau pathology in nontransgenic mice. J Exp Med 213:2635–2654. https://doi.org/10.1084/jem.20160833
37. He Z, Guo JL, McBride JD, Narasimhan S, Kim H, Changolkar L, Zhang B, Gathagan RJ, Yue C, Dengler C, Stieber A, Nitla M, Coulter DA, Abel T, Brunden KR, Trojanowski JQ, Lee VM-Y (2018) Amyloid-β plaques enhance Alzheimer's brain tau-seeded pathologies by facilitating neuritic plaque tau aggregation. Nat Med 24:29–38. https://doi.org/10.1038/nm.4443
38. He Z, McBride JD, Xu H, Changolkar L, Kim S-J, Zhang B, Narasimhan S, Gibbons GS, Guo JL, Kozak M, Schellenberg GD, Trojanowski JQ, Lee VM-Y (2020) Transmission of tauopathy strains is independent of their isoform composition. Nat Commun 11:7. https://doi.org/10.1038/s41467-019-13787-x
39. Holmes BB, Furman JL, Mahan TE, Yamasaki TR, Mirbaha H, Eades WC, Belaygorod L, Cairns NJ, Holtzman DM, Diamond MI (2014) Proteopathic tau seeding predicts tauopathy in vivo. Proc Natl Acad Sci 111:E4376–E4385. https://doi.org/10.1073/pnas.1411649111
40. Iba M, Guo JL, McBride JD, Zhang B, Trojanowski JQ, Lee VM-Y (2013) Synthetic tau fibrils mediate transmission of Neurofibrillary tangles in a transgenic mouse model of Alzheimer's-Like Tauopathy. J Neurosci 33:1024–1037. https://doi.org/10.1523/JNEUROSCI.2642-12.2013
41. Iba M, McBride JD, Guo JL, Zhang B, Trojanowski JQ, Lee VM-Y (2015) Tau pathology spread in PS19 tau transgenic mice following locus coeruleus (LC) injections of synthetic tau fibrils is determined by the LC's afferent and efferent connections. Acta Neuropathol (Berl) 130:349–362. https://doi.org/10.1007/s00401-015-1458-4
42. Jankowski MM, Ronnqvist KC, Tsanov M, Vann SD, Wright NF, Erichsen JT, Aggleton JP, O'Mara SM (2013) The anterior thalamus provides a subcortical circuit supporting memory and spatial navigation. Front Syst Neurosci 7:45. https://doi.org/10.3389/fnsys.2013.00045
43. Kaufman SK, Sanders DW, Thomas TL, Ruchinskas AJ, Vaquer-Alicea J, Sharma AM, Miller TM, Diamond MI (2016) Tau prion strains dictate patterns of Cell Pathology, Progression Rate, and Regional vulnerability in vivo. Neuron 92:796–812. https://doi.org/10.1016/j.neuron.2016.09.055
44. Kumar M, Quittot N, Dujardin S, Schlaffner CN, Viode A, Wiedmer A, Beerepoot P, Chun JE, Glynn C, Fernandes AR, Donahue C, Steen JA, Hyman BT (2024) Alzheimer proteopathic tau seeds are biochemically a forme fruste of mature paired helical filaments. Brain J Neurol awad378. https://doi.org/10.1093/brain/awad378
45. Lasagna-Reeves CA, Castillo-Carranza DL, Sengupta U, Guerrero-Munoz MJ, Kiritoshi T, Neugebauer V, Jackson GR, Kayed R (2012) Alzheimer brain-derived tau oligomers propagate pathology from endogenous tau. Sci Rep 2:700. https://doi.org/10.1038/srep00700
46. Li L, Shi R, Gu J, Tung YC, Zhou Y, Zhou D, Wu R, Chu D, Jin N, Deng K, Xu J, Gong C-X, Iqbal K, Liu F (2021) Alzheimer's disease brain contains tau fractions with differential prion-like activities. Acta Neuropathol Commun 9:28. https://doi.org/10.1186/s40478-021-01127-4
47. Mancuso R, Fryatt G, Cleal M, Obst J, Pipi E, Monzón-Sandoval J, Ribe E, Winchester L, Webber C, Nevado A, Jacobs T, Austin N, Theunis C, Grauwen K, Daniela Ruiz E, Mudher A, Vicente-Rodriguez M, Parker CA, Simmons C, Cash D, Richardson J, Consortium NIMA, Jones DNC, Lovestone S, Gómez-Nicola D, Perry VH (2019) CSF1R inhibitor JNJ-40346527 attenuates microglial proliferation and neurodegeneration in P301S mice. Brain J Neurol 142:3243–3264. https://doi.org/10.1093/brain/awz241
48. De Mate A, Welikovitch LA, Khasnavis A, Commins C, Glynn C, Chun JE, Perbet R, Hyman BT (2023) Tau seeding and spreading in vivo is supported by both AD-derived fibrillar and oligomeric tau. Acta Neuropathol (Berl) 146:191–210. https://doi.org/10.1007/s00401-023-02600-1
49. Mirbaha H, Chen D, Morazova OA, Ruff KM, Sharma AM, Liu X, Goodarzi M, Pappu RV, Colby DW, Mirzaei H, Joachimiak LA, Diamond MI (2018) Inert and seed-competent tau monomers suggest structural origins of aggregation. eLife 7. https://doi.org/10.7554/eLife.36584
50. Narasimhan S, Guo JL, Changolkar L, Stieber A, McBride JD, Silva LV, He Z, Zhang B, Gathagan RJ, Trojanowski JQ, Lee VMY (2017) Pathological tau strains from human brains recapitulate the Diversity of Tauopathies in Nontransgenic Mouse Brain. J Neurosci 37:11406–11423. https://doi.org/10.1523/JNEUROSCI.1230-17.2017
51. Narasimhan S, Lee VMY (2017) The use of mouse models to study cell-to-cell transmission of pathological tau. Methods Cell Biol 141:287–305. https://doi.org/10.1016/bs.mcb.2017.06.009
52. Ohara S, Rannap M, Tsutsui K-I, Draguhn A, Egorov AV, Witter MP (2023) Hippocampal-medial entorhinal circuit is differently organized along the dorsoventral axis in rodents. Cell Rep 42:112001. https://doi.org/10.1016/j.celrep.2023.112001
53. Peeraer E, Bottelbergs A, Van Kolen K, Stancu I-C, Vasconcelos B, Mahieu M, Duytschaever H, Ver Donck L, Torremans A, Sluydts E, Van Acker N, Kemp JA, Mercken M, Brunden KR, Trojanowski JQ, Dewachter I, Lee VMY, Moechars D (2015) Intracerebral injection of preformed synthetic tau fibrils initiates widespread tauopathy and neuronal loss in the brains of tau transgenic mice. Neurobiol Dis 73:83–95. https://doi.org/10.1016/j.nbd.2014.08.032
54. Prusiner SB (1982) Novel proteinaceous infectious particles cause scrapie. Science 216:136–144
55. Saito T, Mihira N, Matsuba Y, Sasaguri H, Hashimoto S, Narasimhan S, Zhang B, Murayama S, Higuchi M, Lee VMY, Trojanowski JQ, Saido TC (2019) Humanization of the entire murine mapt gene provides a murine model of pathological human tau propagation. J Biol Chem 294:12754–12765. https://doi.org/10.1074/jbc.RA119.009487
56. Sanders DW, Kaufman SK, DeVos SL, Sharma AM, Mirbaha H, Li A, Barker SJ, Foley A, Thorpe JR, Serpell LC, Miller TM, Grinberg LT, Seeley WW, Diamond MI (2014) Distinct tau prion strains propagate in cells and mice and define different tauopathies. Neuron 82:1271–1288. https://doi.org/10.1016/j.neuron.2014.04.047
57. Sato C, Barthélemy NR, Mawuenyega KG, Patterson BW, Gordon BA, Jockel-Balsarotti J, Sullivan M, Crisp MJ, Kasten T, Kirmess KM, Kanaan NM, Yarasheski KE, Baker-Nigh A, Benzinger TLS, Miller TM, Karch CM, Bateman RJ (2018) Tau kinetics in neurons and the Human Central Nervous System. Neuron 97:1284–1298e7. https://doi.org/10.1016/j.neuron.2018.02.015
58. Serrano-Pozo A, Frosch MP, Masliah E, Hyman BT (2011) Neuropathological alterations in Alzheimer disease. Cold Spring Harb Perspect Med 1:a006189. https://doi.org/10.1101/cshperspect.a006189
59. Sethumadhavan N, Strauch C, Hoang T-H, Manahan-Vaughan D (2022) The Perirhinal Cortex engages in Area and Layer-Specific Encoding of Item dimensions. Front Behav Neurosci 15
60. Shi Y, Zhang W, Yang Y, Murzin AG, Falcon B, Kotecha A, van Beers M, Tarutani A, Kametani F, Garringer HJ, Vidal R, Hallinan GI, Lashley T, Saito Y, Murayama S, Yoshida M, Tanaka H, Kakita A, Ikeuchi T, Robinson AC, Mann DMA, Kovacs GG, Revesz T, Ghetti B, Hasegawa M, Goedert M, Scheres SHW (2021) Structure-based classification of tauopathies. Nature 598:359–363. https://doi.org/10.1038/s41586-021-03911-7
61. Song L, Oseid DE, Wells EA, Robinson AS (2022) The interplay between GSK3β and tau Ser262 phosphorylation during the Progression of Tau Pathology. Int J Mol Sci 23:11610. https://doi.org/10.3390/ijms231911610
62. Stefanoska K, Gajwani M, Tan ARP, Ahel HI, Asih PR, Volkerling A, Poljak A, Ittner A (2022) Alzheimer's disease: ablating single master site abolishes tau hyperphosphorylation. Sci Adv 8:eabl8809. https://doi.org/10.1126/sciadv.abl8809
63. Taddei RN, Sanchez-Mico MV, Bonnar O, Connors T, Gaona A, Denbow D, Frosch MP, Gómez-Isla T (2022) Changes in glial cell phenotypes precede overt neurofibrillary tangle formation, correlate with markers of cortical cell damage, and predict cognitive status of individuals at Braak III-IV stages. Acta Neuropathol Commun 10:72. https://doi.org/10.1186/s40478-022-01370-3

64. Takeda S, Wegmann S, Cho H, DeVos SL, Commins C, Roe AD, Nicholls SB, Carlson GA, Pitstick R, Nobuhara CK, Costantino I, Frosch MP, Müller DJ, Irimia D, Hyman BT (2015) Neuronal uptake and propagation of a rare phosphorylated high-molecular-weight tau derived from Alzheimer's disease brain. Nat Commun 6:8490. https://doi.org/10.1038/ncomms9490
65. Thal DR, Rüb U, Orantes M, Braak H (2002) Phases of a beta-deposition in the human brain and its relevance for the development of AD. Neurology 58:1791–1800. https://doi.org/10.1212/wnl.58.12.1791
66. Tok S, Maurin H, Delay C, Crauwels D, Manyakov NV, Van Der Elst W, Moechars D, Drinkenburg WHIM (2022) Pathological and neurophysiological outcomes of seeding human-derived tau pathology in the APP-KI NL-G-F and NL-NL mouse models of Alzheimer's Disease. Acta Neuropathol Commun 10:92. https://doi.org/10.1186/s40478-022-01393-w
67. Vaquer-Alicea J, Diamond MI, Joachimiak LA (2021) Tau strains shape disease. Acta Neuropathol (Berl). https://doi.org/10.1007/s00401-021-02301-7
68. Vergara C, Houben S, Suain V, Yilmaz Z, De Decker R, Vanden Dries V, Boom A, Mansour S, Leroy K, Ando K, Brion J-P (2019) Amyloid-β pathology enhances pathological fibrillary tau seeding induced by Alzheimer PHF in vivo. Acta Neuropathol (Berl) 137:397–412. https://doi.org/10.1007/s00401-018-1953-5
69. Welikovitch LA, Dujardin S, Dunn AR, Fernandes AR, Khasnavis A, Chibnik LB, Kaczorowski CC, Hyman BT (2023) Rate of tau propagation is a heritable disease trait in genetically diverse mouse strains. iScience 26:105983. https://doi.org/10.1016/j.isci.2023.105983
70. Wesseling H, Mair W, Kumar M, Schlaffner CN, Tang S, Beerepoot P, Fatou B, Guise AJ, Cheng L, Takeda S, Muntel J, Rotunno MS, Dujardin S, Davies P, Kosik KS, Miller BL, Berretta S, Hedreen JC, Grinberg LT, Seeley WW, Hyman BT, Steen H, Steen JA (2020) Tau PTM profiles identify patient heterogeneity and stages of Alzheimer's Disease. Cell 183:1699–1713e13. https://doi.org/10.1016/j.cell.2020.10.029
71. Wu R, Li L, Shi R, Zhou Y, Jin N, Gu J, Tung YC, Liu F, Chu D (2021) Dephosphorylation passivates the seeding activity of oligomeric tau derived from Alzheimer's brain. Front Mol Neurosci 14:631833. https://doi.org/10.3389/fnmol.2021.631833

Publisher's Note